Ion mass dependence of irradiation-induced local creation of ferromagnetism in $Fe_{60}Al_{40}$ alloys

J. Fassbender,* M. O. Liedke, T. Strache, and W. Möller
Institute of Ion Beam Physics and Materials Research, Forschungszentrum Dresden-Rossendorf, P.O. Box 51 01 19, 01314 Dresden, Germany

E. Menéndez
Departament de Física, Universitat Autònoma de Barcelona, 08193 Bellaterra, Spain

J. Sort
Institució Catalana de Recerca i Estudis Avançats (ICREA) and Departament de Física, Universitat Autònoma de Barcelona, 08193 Bellaterra, Spain

K. V. Rao
Department of Materials Science and Engineering, Royal Institute of Technology, S-10044 Stockholm, Sweden

S. C. Deevi
Research Center, Chrysalis Technologies Incorporated, Richmond, Virginia 23234, USA

J. Nogués
Institució Catalana de Recerca i Estudis Avançats (ICREA) and Institut Català de Nanotecnologia, Edifici CM7, Campus Universitat Autònoma de Barcelona, 08193 Bellaterra, Spain

(Received 5 October 2007; revised manuscript received 27 March 2008; published 28 May 2008)

Ion irradiation of $Fe_{60}Al_{40}$ alloys results in the phase transformation from the *paramagnetic*, chemically ordered B2 phase to the *ferromagnetic*, chemically disordered A2 phase. The magnetic phase transformation is related to the number of displacements per atom (dpa) during the irradiation. For heavy ions (Ar^+, Kr^+, and Xe^+), a universal curve is observed with a steep increase in the fraction of the ferromagnetic phase that reaches saturation, i.e., a complete phase transformation, at about 0.5 dpa. This proves the purely ballistic nature of the disordering process. If light ions are used (He^+ and Ne^+), a pronounced deviation from the universal curve is observed. This is attributed to bulk vacancy diffusion from the dilute collision cascades, which leads to a partial recovery of the thermodynamically favored B2 phase. Comparing different noble gas ion irradiation experiments allows us to assess the corresponding counteracting contributions. In addition, the potential to create local ferromagnetic areas embedded in a paramagnetic matrix is demonstrated.

DOI: 10.1103/PhysRevB.77.174430 PACS number(s): 75.50.Bb, 61.80.Jh, 75.30.Kz

The patterning of magnetic materials has become of utmost importance during the last two decades due to the potential applications in magnetic data storage and for magnetologic devices. In addition to standard top-down lithographic approaches, bottom-up self-assembly procedures are also currently widely investigated in order to achieve maximum packing densities.[1] However, for many applications, the topography associated with the patterning is detrimental. Therefore, a pure magnetic patterning, which leaves the surface unaffected, is highly desirable. In recent years, ion irradiation has been established as a powerful tool to modify and tailor the magnetic properties of thin magnetic films and multilayered structures. Most of the examples known so far rely on the fact that the magnetic properties sensitively depend on the interface structure,[2] i.e., the perpendicular anisotropy in Co/Pt (Ref. 3) and the exchange bias in bilayers of ferromagnetic and antiferromagntic films[4] or the interlayer exchange coupling such as in Fe/Cr/Fe trilayers.[5] In order to modify single ferromagnetic layers, which are much less sensitive to interface effects, different routes can be employed: (i) a change in composition either by direct implantation[6] or by irradiation-induced mixing with cap and buffer layers,[7] (ii) a change in short range order in alloy films in order to modify the uniaxial anisotropy direction,[8] or (iii) a change in the chemical ordering in alloys.[9–12] The best investigated system in the latter case is FePt (Refs. 9–11). Here, due to light ion irradiation, an increase in the magnetic anisotropy is achieved that originates from a phase transformation from the chemically disordered fcc phase to the chemically ordered $L1_0$ phase. This rather counterintuitive process was explained by Bernas *et al.*[10] by an irradiation enhanced diffusion mechanism that provides a route to a thermodynamically favored $L1_0$ phase, which is otherwise kinetically impeded. If this process is combined with lithographic techniques, a magnetic composite material comprising hard and soft magnetic areas can be created. The reverse process, i.e., a transformation from the chemically ordered (here, $L1_2$) to the chemically disordered phase has been observed upon 700 keV N^+ ion irradiation of $CrPt_3$ (Ref. 12) and $FePt_3$ (Ref. 13). The corresponding magnetic properties change from ferrimagnetic to nonmagnetic[12] and from antiferromagnetic to ferromagnetic,[13] respectively. However, so far, no systematic investigations on the disordering efficiency of different ion species have been reported.

It is experimentally and theoretically established that $Fe_{60}Al_{40}$ alloys are paramagnetic in a thermodynamically

stable chemically ordered B2 phase, while they are ferromagnetic in the metastable disordered A2 phase.[14,15] Conventionally, the metastable A2 phase is established by a mechanical deformation (e.g., ball milling).[15] An interesting local approach is presented by Sort *et al.*[16] by means of nanoindentation. In this study, it was possible to create periodic arrays of submicrometer ferromagnetic structures. However, in this approach, a variation in the structure shape is difficult to obtain and a change in the surface topography is inevitable. In this respect, the creation of ferromagnetism by means of local ion irradiation, as presented in the following, offers considerable advantages. Potential applications are patterned storage media or servo track patterns for read head positioning.[17]

In the present report, the local creation of ferromagnetism in a paramagnetic chemically B2-ordered $Fe_{60}Al_{40}$ alloy by ion irradiation is described for irradiation at varying ion species and energy and related to ion-induced lattice damage. The counteracting processes of ballistic mixing and vacancy diffusion induced recovery of the thermodynamically favored B2 phase are addressed. In addition, it is demonstrated that micropatterning can be achieved by homogeneous ion irradiation through a mask.

Bulk $Fe_{60}Al_{40}$ sheets with 250-μm thickness have been prepared by repeated cold rolling and annealing by using a recipe described elsewhere.[18] Subsequently, the sheets have been mechanically polished and annealed to 900 K for 20 min in order to remove any magnetic contributions that might have been introduced during the preparation process. For the irradiations, a DANFYSIK low-energy ion implanter has been used. The primary energy of the different ions (2 keV He^+, 11 keV Ne^+, 21 keV Ar^+, 35 keV Kr^+, and 45 keV Xe^+) was adjusted to position the maximum of the collisional damage distribution at a depth of 10 nm.[19] The ion fluence has been varied to obtain an average damage within the top 20 nm of 0.05–5 dpa (displacement per atom). In order to exclude any ion flux effects, which might arise from an interplay of ion bombardment and thermal diffusion (see below), the ion current density was varied from 0.02 (for Xe^+) to 2 $\mu A/cm^2$ (for He^+) to achieve the same average damage rate for all ion species. The structure of the modified surface layer has been investigated by glancing incidence x-ray diffraction (GIXRD) using a Siemens D5005 diffractometer with Cu $K\alpha_1$ ($\lambda=0.15406$ nm) radiation with a fixed incident angle of 1°. The microstructural parameters (crystallite sizes, average coherently diffracting domain sizes, microstrains, atomic level deformations, lattice parameters, and atomic occupancies) were evaluated by adjusting the spectra by means of a full pattern fitting RIETVELD program.[20] For a proof of principle in a patterning experiment, a 2 000 mesh grid (with a 7.5×7.5 μm^2 mesh size, 12.5 μm pitch, and 20 μm thickness) was employed. The magnetic characterization has been performed by a longitudinal magneto-optic Kerr effect (MOKE) magnetometry and magnetic force microscopy (MFM).

In Fig. 1, the hysteresis loops are shown as obtained before and after 45 keV Xe^+ irradiation for different fluences and thereby damage levels. As expected, prior to ion irradiation, no ferromagnetic behavior is detectable. Interestingly, a rather low Xe^+ fluence of 10^{13} ions/cm^2 already leads to a

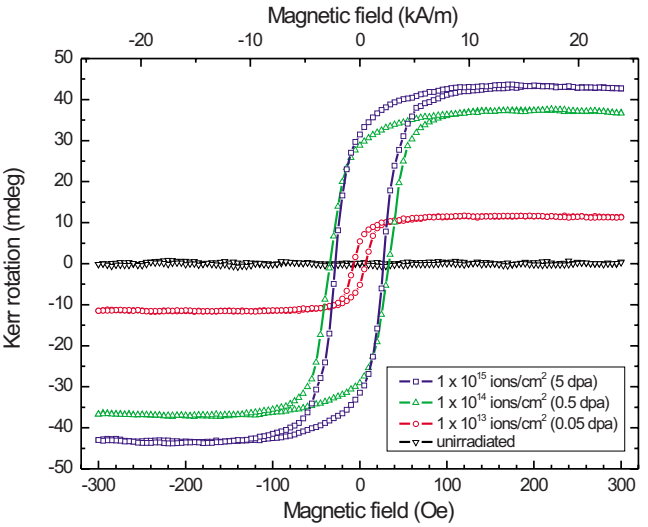

FIG. 1. (Color online) Hysteresis loops investigated by means of longitudinal magneto-optic Kerr effect of an $Fe_{60}Al_{40}$ alloy before and after being irradiated with three different fluences of 45 keV Xe^+. In addition, the average damage within a depth of 20 nm is specified.

substantial ferromagnetic signal with the hysteresis loop exhibiting a coercive field of 7 Oe. The transformation to the ferromagnetic state in the near-surface region saturates at a damage level well above 0.5 dpa.[21] Thus, at 0.05 dpa about 30 vol % of that region has already turned to ferromagnetic. Remarkably, at a sputter yield of 7.5 atoms/ion, the irradiation-induced erosion is below 0.1 monolayer at such a low fluence. For 0.5 dpa, the coercivity increases to 35 Oe, and the squareness improves to $M_R/M_S=0.75$ (where M_R and M_S are the remanent magnetization and the saturation magnetization, respectively). At this fluence, the sputtering is still less than one monolayer. No significant in-plane anisotropy could be detected by measuring the hysteresis curves as a function of the in-plane angle (not shown). This corresponds to the random orientation of the grains in the sheet. Increasing the average damage to 5 dpa results in only a slight reduction in coercive field and squareness. The subsequent annealing of the sample to 800 K for 30 min completely restores the initial paramagnetic state (not shown). These results demonstrate the feasibility to generate *ferromagnetic* phases from *paramagnetic* ones by ion irradiation, which are in contrast to other systems that were investigated so far, where mostly the contrary effect (ferromagnetic $\rightarrow$paramagnetic, i.e, the destruction of magnetism) has been shown.

In order to further quantify the evolution of the ferromagnetic phase, the amplitude of the MOKE signal, which is a measure of the magnetic moment, is shown in Fig. 2(a) as a function of the fluence of different ions (note the logarithmic scale). As expected, at a lower ion mass, a larger ion fluence is required to obtain the same magnetic moment. For example, to obtain the same MOKE amplitude, the irradiation fluence for He^+ is about 3 orders of magnitude larger than for Xe^+. Although the already quite high He^+ irradiation fluences are used, a surface blistering was not observed. Nevertheless, subsurface void formation is likely indicated by hysteresis

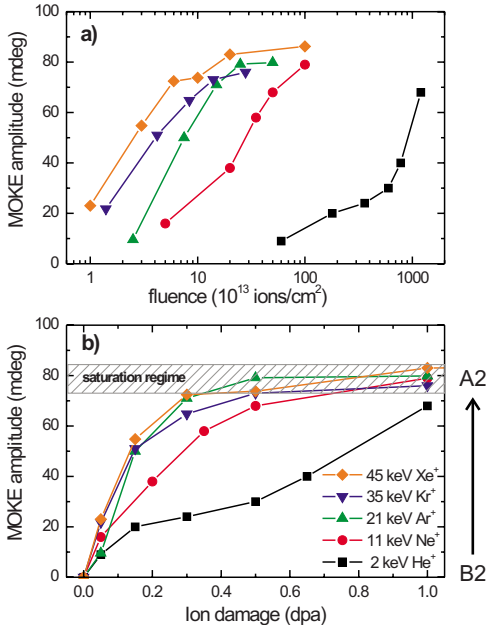

FIG. 2. (Color online) MOKE amplitude (a) as a function of ion fluence and (b) as a function of ion damage for five different ion species (He^+, Ne^+, Ar^+, Kr^+, and Xe^+). The primary energy is adjusted to achieve the maximum number of displacements per atom in a 10 nm depth of the $Fe_{60}Al_{40}$ alloy. The irradiation causes the transition from the paramagnetic B2 structure to the ferromagnetic A2 structure.

measurements after annealing steps (not shown). If the high fluence He^+ and Xe^+ irradiated samples are compared, for Xe^+ irradiation lower annealing temperatures are sufficient to reestablish the original paramagnetic state. If the MOKE amplitude is plotted versus the damage [see Fig. 2(b)], the data spread is considerably reduced and a universal behavior is observed for the heavy ion species Ar^+, Kr^+, and Xe^+. As mentioned above, at about 0.5 dpa, the saturation regime of the ferromagnetic behavior is reached, which indicates that the phase transformation to the disordered A2 phase in the near-surface region due to the ballistic mixing processes is completed. However, for lighter ions, a distinct deviation from this universal curve is observed, i.e., a significantly larger nominal damage is required to induce the transition. This can be explained by the different topologies of the collision cascades that is associated with different ion masses, which can be visualized by TRIM computer simulation.[19] Light ions tend to create dilute vacancy-interstitial pairs along the ion track, which are essentially all available for diffusion into the surrounding matrix with the mobile vacancies leading to chemical reordering in the environment as mentioned above. On the other hand, heavy ions develop sequences of spatially dense collision subcascades with a high probability of dynamic annealing within the subcascades.[22] Thus, at equal nominal damage, less mobile vacancies will be available and consequently, less reordering will occur in comparison to light ions. Furthermore, the dense subcascades, which are preferentially generated by heavier ions, may result in local regions where the chemical order is lost, which is in analogy to amorphous pockets found in semiconductors.[23] These regions might be more resistant to reordering than the isolated defects that are preferentially created during light ion irradiation. Hence, while ballistic mixing arguments satisfactorily explain heavy ion irradiation effects, a dynamic recovery of thermodynamically stable phases always has to be considered for light ion irradiation.

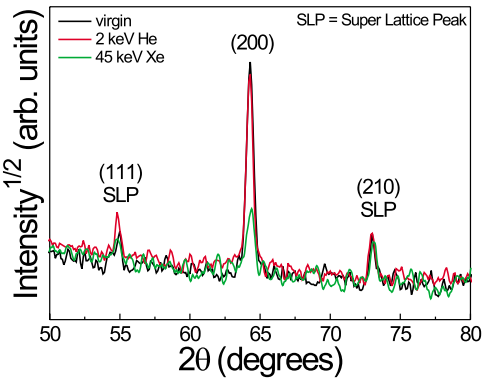

FIG. 3. (Color online) The GIXRD spectra of the $Fe_{60}Al_{40}$ (at. %) alloy after being annealed (i.e., virgin) and homogeneously irradiated by using either He^+ (2 keV, 0.2 dpa) or Xe^+ (45 keV, 0.3 dpa). The Miller indices of the $Fe_{60}Al_{40}$ (at. %) alloy are also indicated. Note that SLPs denote the superlattice peaks.

In order to further support the above interpretation, GIXRD has been used to investigate the virgin sample and two irradiated samples (He^+ and Xe^+) with a similar damage level (0.2–0.3 dpa). In this range, the difference between magnetic signals is maximal. Note that the GIXRD signal is always a superposition of the modified top 20 nm and the unaffected bulk beneath. However, analyzing the GIXRD data (see Fig. 3) in detail leads to the parameters given in Table I. Similarly, the damage levels of Xe^+ irradiation, in comparison to He^+ irradiation, leads to a stronger reduction in the long-range order parameter S and a stronger increase in lattice spacing a. Since both are required in order to achieve ferromagnetic order, these are consistent with the stronger ferromagnetic signal for Xe^+ irradiation. A remarkable analogy is found if ion irradiation-induced amorphization of metallic alloys is considered.[24] In these investigations, the resistivity, which is a measure of the amorphized fraction, exhibits a similar course as a function of ion fluence and also displays a distinct difference if light or heavy ions are used. This proves that the concept of the collision cascade topology can be applied in a wider range of experiments to explain various ion irradiation-induced phenomena.

Finally, we demonstrate the parallel generation of ferro-

TABLE I. Summary of parameters determined from GIXRD and MOKE for the virgin as well as the He^+ or Xe^+ irradiated samples.

$Fe_{60}Al_{40}$ (at. %)	Virgin	He^+	Xe^+
Damage (dpa)	0	0.2	0.3
Long-range order parameter S	0.66	0.52	0.34
Lattice spacing a (Å)	2.8977	2.8985	2.8995
MOKE amplitude (mdeg)	0	23	73

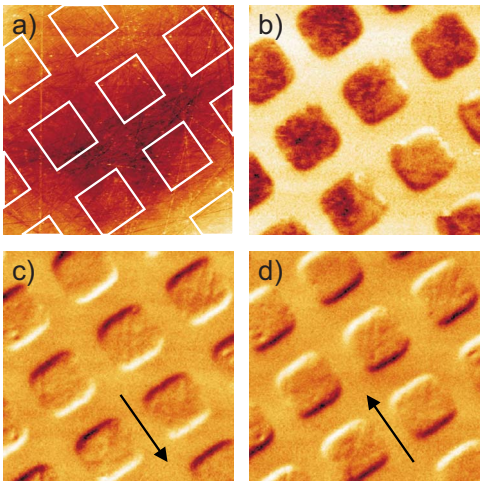

FIG. 4. (Color online) (a) AFM and [(b)–(d)] MFM images of the FeAl sheet after Xe^+ irradiation. The squares in (a) indicate the 7.5×7.5 μm^2 regions that have been irradiated. For the series of MFM images, different magnetic fields have been applied: (b) 0 Oe, (c) −400 Oe, and (d) 400 Oe. The arrows in (c) and (d) indicate the direction of the applied magnetic field.

magnetic arrays over large areas (typically over square millimeters) by means of this technique. For this purpose, broad beam irradiation through a grid, which is used as a mask, has been performed. In Fig. 4(a), an atomic force microscopy (AFM) image of the FeAl sheet is shown. No change in topography is observed after irradiation. In Figs. 4(b)–4(d), the corresponding MFM images acquired in different applied in-plane magnetic fields are shown. If a magnetic field of ±400 Oe is applied, which is sufficient to saturate the magnetization (cf. Fig. 1), single-domain ferromagnetic regions are nicely observed by the stray field contrast at the boundaries of the embedded ferromagnets. The magnetic origin of the contrast is proven by the stray field reversal upon magnetic field reversal [see Figs. 4(c) and 4(d)]. If no magnetic field is applied, the single domain state decomposes into multidomain states [Fig. 4(b)]. However, some remanent magnetization remains, which is consistent with the hysteresis loops shown in Fig. 1. In order to achieve a single domain behavior, also in the remanent state, the ferromagnetic features have to be shrunk in size. In general, this is possible by making use of stencil masks with local irradiation areas in the range of 100 nm (Ref. 25). By using this technique, further miniaturization is also straightforward and would allow parallel production of nanomagnets within a couple of seconds.

In summary, the effect of different ion masses on the disordering efficiency of chemically ordered $Fe_{60}Al_{40}$ alloys is enlightened. For heavy ions, a pure ballistic mixing occurs, which is reflected by a universal curve for the damage dependence of the induced magnetism. However, for light ions, a dynamic recovery of the thermodynamically stable phase, which reduces the disordering efficiency, has to be taken into account. In addition, the viability of magnetic patterning potential is shown.

The authors thank K.-H. Heinig for the valuable discussions and I. Winkler for the technical help with the ion irradiation. This work was partially supported by the EU—"Research Infrastructures Transnational Access" program "Center for Application of Ion Beams in Materials Research" under Contract No. 025646, DFG project FA 314/3-1, Catalan DGR Project No. 2005SGR-00401, Spanish CICYT Projects No. MAT-2007-66302-C02 and No. MAT-2007-61629, and the Institut Català de Nanotecnologia (ICN).

*j.fassbender@fzd.de

[1] J. I. Martín, J. Nogués, K. Liu, J. L. Vicent, and I. K. Schuller, J. Magn. Magn. Mater. **256**, 449 (2003).

[2] For a recent overview, see, J. Fassbender, D. Ravelosona, and Y. Samson, J. Phys. D **37**, R179 (2004); J. Fassbender and J. McCord, J. Magn. Magn. Mater. **320**, 579 (2008).

[3] C. Chappert, H. Bernas, J. Ferre, V. Kottler, J. P. Jamet, Y. Chen, E. Cambril, T. Devolder, F. Rousseaux, V. Mathet, and H. Launois, Science **280**, 1919 (1998); T. Devolder, C. Chappert, Y. Chen, E. Cambril, H. Bernas, J. P. Jamet, and J. Ferre, Appl. Phys. Lett. **74**, 3383 (1999).

[4] T. Mewes, R. Lopusnik, J. Fassbender, B. Hillebrands, M. Jung, D. Engel, A. Ehresmann, and H. Schmoranzer, Appl. Phys. Lett. **76**, 1057 (2000); A. Mougin, T. Mewes, M. Jung, D. Engel, A. Ehresmann, H. Schmoranzer, J. Fassbender, and B. Hillebrands, Phys. Rev. B **63**, 060409(R) (2001).

[5] S. O. Demokritov, C. Bayer, S. Poppe, M. Rickart, J. Fassbender, B. Hillebrands, D. I. Kholin, N. M. Kreines, and O. M. Liedke, Phys. Rev. Lett. **90**, 097201 (2003); S. Blomeier, P. Candeloro, B. Hillebrands, B. Reuscher, A. Brodyanski, and M. Kopnarski, Phys. Rev. B **74**, 184405 (2006).

[6] L. Folks, R. E. Fontana, B. A. Gurney, J. R. Childress, S. Maat, J. A. Katine, J. E. E. Baglin, and A. J. Kellock, J. Phys. D **36**, 2601 (2003); J. Fassbender, J. von Borany, A. Mucklich, K. Potzger, W. Möller, J. McCord, L. Schultz, and R. Mattheis, Phys. Rev. B **73**, 184410 (2006).

[7] M. Albrecht, C. T. Rettner, M. E. Best, and B. D. Terris, Appl. Phys. Lett. **83**, 4363 (2003); D. McGrouther and J. N. Chapman, *ibid.* **87**, 022507 (2005); J. Fassbender and J. McCord, *ibid.* **88**, 252501 (2006); B. S. Pang, Y. J. Chen, and S. H. Leong, *ibid.* **88**, 094103 (2006).

[8] S. I. Woods, S. Ingvarsson, J. R. Kirtley, H. F. Hamann, and R. H. Koch, Appl. Phys. Lett. **81**, 1267 (2002); J. McCord, T. Gemming, L. Schultz, J. Fassbender, M. O. Liedke, M. Frommberger, and E. Quandt, *ibid.* **86**, 162502 (2005).

[9] D. Ravelosona, C. Chappert, V. Mathet, and H. Bernas, Appl. Phys. Lett. **76**, 236 (2000); C.-H. Lai, C.-H. Yang, and C. C. Chiang, *ibid.* **83**, 4550 (2003).

[10] H. Bernas, J. P. Attane, K. H. Heinig, D. Halley, D. Ravelosona, A. Marty, P. Auric, C. Chappert, and Y. Samson, Phys. Rev. Lett. **91**, 077203 (2003).

[11] U. Wiedwald, A. Klimmer, B. Kern, L. Han, H. G. Boyen, P. Ziemann, and K. Fauth, Appl. Phys. Lett. **90**, 062508 (2007).

[12] O. Hellwig, D. Weller, A. J. Kellock, J. E. E. Baglin, and E. E.

Fullerton, Appl. Phys. Lett. **79**, 1151 (2001).
[13] S. Maat, A. J. Kellock, D. Weller, J. E. E. Baglin, and E. E. Fullerton, J. Magn. Magn. Mater. **265**, 1 (2003).
[14] J. Bogner, W. Steiner, M. Reissner, P. Mohn, P. Blaha, K. Schwarz, R. Krachler, H. Isper, and B. Sepiol, Phys. Rev. B **58**, 14922 (1998); N. I. Kulikov, A. V. Postnikov, G. Borstel, and J. Braun, *ibid.* **59**, 6824 (1999); E. Apiñaniz, F. Plazaola, and J. S. Garitaonandia, Eur. Phys. J. B **31**, 167 (2003).
[15] A. Hernando, X. Amils, J. Nogués, S. Suriñach, M. D. Baró, and M. R. Ibarra, Phys. Rev. B **58**, R11864 (1998); X. Amils, J. Nogués, S. Suriñach, J. S. Muñoz, M. D. Baró, A. Hernando, and J. P. Morniroli, *ibid.* **63**, 052402 (2001); Q. Zeng and I. Baker, Intermetallics **14**, 396 (2006); J. Nogués, E. Apiñaniz, J. Sort, M. Amboage, M. d'Astuto, O. Mathon, R. Puzniak, I. Fita, J. S. Garitaonandia, S. Suriñach, J. S. Muñoz, M. D. Baró, F. Plazaola, and F. Baudelet, Phys. Rev. B **74**, 024407 (2006).
[16] J. Sort, A. Concustell, E. Menéndez, S. Suriñach, K. V. Rao, S. C. Deevi, M. D. Baró, and J. Nogués, Adv. Mater. (Weinheim, Ger.) **18**, 1717 (2006).
[17] B. D. Terris and T. Thomson, J. Phys. D **38**, R199 (2005).
[18] D. G. Morris and S. C. Deevi, Mater. Sci. Eng., A **329-331**, 573 (2002).
[19] The calculations have been performed by using the SRIM 2003 code, J. F. Ziegler, J. P. Biersack, and U. Littmark, *The Stopping and Range of Ions in Solids* (Pergamon, New York, 1985).
[20] L. Lutterotti and P. Scardi, J. Appl. Crystallogr. **23**, 246 (1990); R. A. Young, *The Rietveld Method (International Union of Crystallography)* (University Press, Oxford, 1995).
[21] Note that the magnetization directly scales with the degree of chemical disorder (cf. Ref. 15).
[22] This is reflected by the concept of the so-called cascade efficiency, which varies between ~0.3 and 1 for heavy and light ions, respectively; see R. S. Averback, R. Benedek, and K. L. Merkle, J. Nucl. Mater. **69&70**, 786 (1978). Although the energies covered in the cited reference are significantly larger, this is expected to be valid as long as the maximum energy transfer in primary collisions is large compared to the damage threshold energy.
[23] M.-J. Caturla, T. Diaz de la Rubia, L. A. Marques, and G. H. Gilmer, Phys. Rev. B **54**, 16683 (1996); J. Nord, K. Nordlund, and J. Keinonen, *ibid.* **65**, 165329 (2002).
[24] P. Ziemann, W. Miehle, and A. Plewnia, Nucl. Instrum. Methods Phys. Res. B **80-81**, 370 (1993).
[25] B. D. Terris, L. Folks, D. Weller, J. E. E. Baglin, A. J. Kellock, H. Rothuizen, and P. Vettiger, Appl. Phys. Lett. **75**, 403 (1999).